Supporting Information

Technique for real-time measurements of endothelial permeability in a microfluidic membrane chip using laser-induced fluorescence detection

Edmond W.K. Young[a,b,†], Michael W.L. Watson[c], Suthan Srigunapalan[a,b], Aaron R. Wheeler*[b,c], Craig A. Simmons*[a,b]

[a] Department of Mechanical & Industrial Engineering, University of Toronto, 5 King's College Road, Toronto, Ontario, M5S 3G8

[b] Institute of Biomaterials & Biomedical Engineering, University of Toronto, 164 College Street, Toronto, Ontario M5S 3G9

[c] Department of Chemistry, University of Toronto, 80 St. George St., Toronto, Ontario, M5S 3H6

† Current location: Department of Biomedical Engineering, University of Wisconsin-Madison, Wisconsin Institutes for Medical Research, 1111 Highland Avenue, Madison, WI, USA, 53705

*co-corresponding authors

email: simmons@mie.utoronto.ca

Tel: 416-946-0548

Fax: 416-978-7753

email: awheeler@chem.utoronto.ca

Tel: 416-946-3864

Fax: 416-946-3865

Abstract

The supporting information contains a figure describing the procedure used to test and characterize the membrane microfluidic devices prior to permeability testing. The figure is important for demonstrating how devices were tested for potential leakages before use. In addition, a derivation of the cylindrical pore flow model for comparing theoretical predictions to measured permeability is included for completeness. We also provide a table that summarizes the main parameters used for the reported experiments, along with measurements taken of the membrane pores that were used to accurately estimate the theoretical permeability of an untreated PET membrane.

Testing Membrane Permeability and Device Leakage

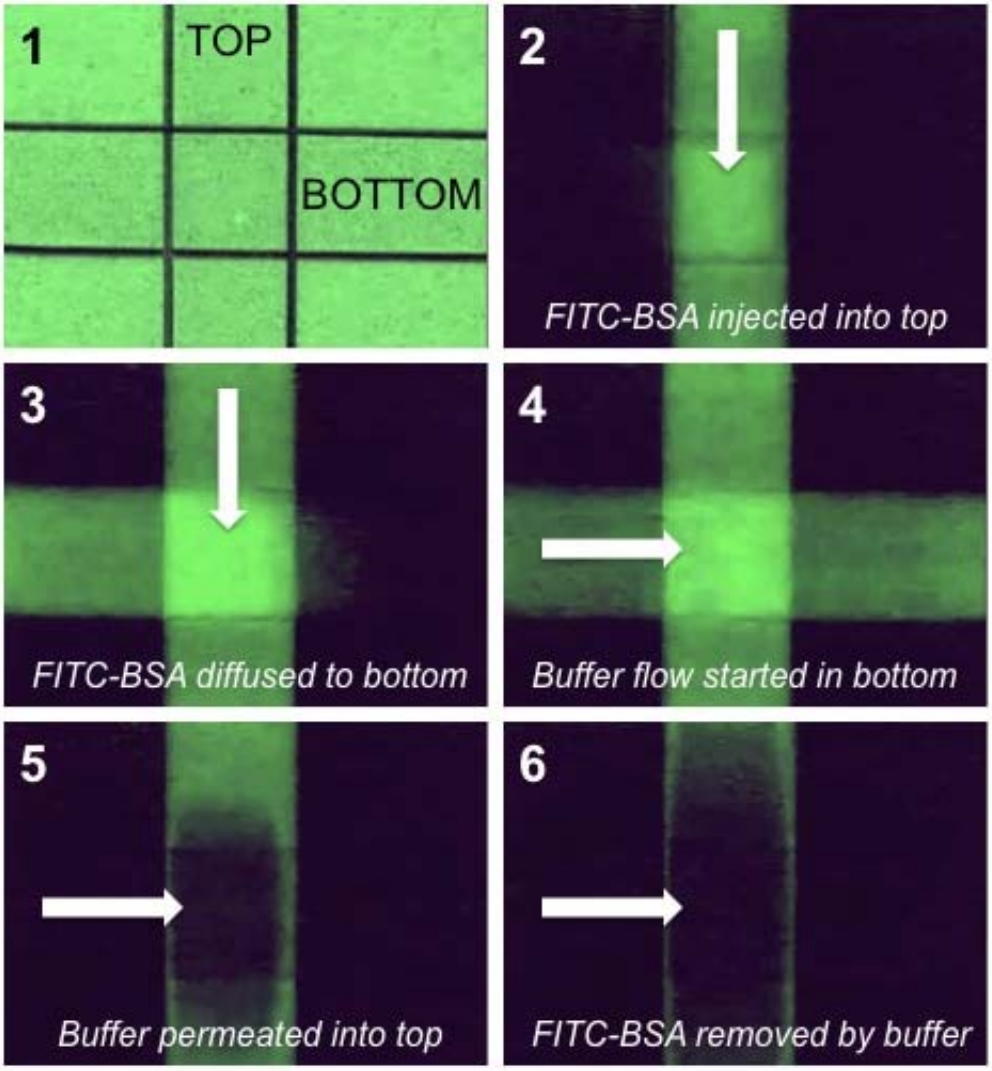

Figure S-1. (1) Phase contrast image of microchannel intersection. (2) FITC-BSA was injected into top channel. (3) FITC-BSA permeated into bottom channel. (4) Flow in bottom channel was started. (5) Buffer was allowed to wash the permeated BSA downstream of intersection. (6) Buffer then permeated membrane from bottom channel to top channel, thus removing the BSA in top channel.

Model for Permeability Measurement by LIF Detection

We provide a detailed derivation of the model used to predict permeability of porous layers based on measurements from laser-induced fluorescence detection. Using our approach, we demonstrate that the model predicts permeability through an uncoated acellular PET membrane to within 1% of experimental measurements.

The problem of interest, as illustrated in Figure 1 of the main text and Figure S-1 below, involves the flux of solute molecules, J_p, through a porous layer from a concentrated top microchannel to a lower buffered microchannel initially free of solute molecules. Solute flux through porous materials is governed by:

$$J_p = -f_d D_s \frac{\partial c}{\partial z} + f_c v_p c \qquad \text{(S.1)}$$

where the first and second terms on the right hand side represent the diffusive and convective flux components, respectively. In Eq. (S.**1**), D_s is diffusivity of the solute; v_p is the fluid pore velocity; and f_d and f_c represent the ratios of flux through porous media to that of flux in free solution for the diffusive and convective terms.[1] These two factors are specific to transport in porous media, and account for pore geometry, steric and viscous effects (described below), and other secondary considerations that affect mass transport in porous materials. In free solution, f_d and f_c are both unity, and solute flux simplifies to $J_p = -D_s \partial c/\partial z + v_p c$, as expected. If we assume that the flux J_p is constant through the thickness of a (thin) porous layer, Eq. (S.**1**) can be solved for solute concentration in the direction of porous flow (i.e., the *z*-direction):

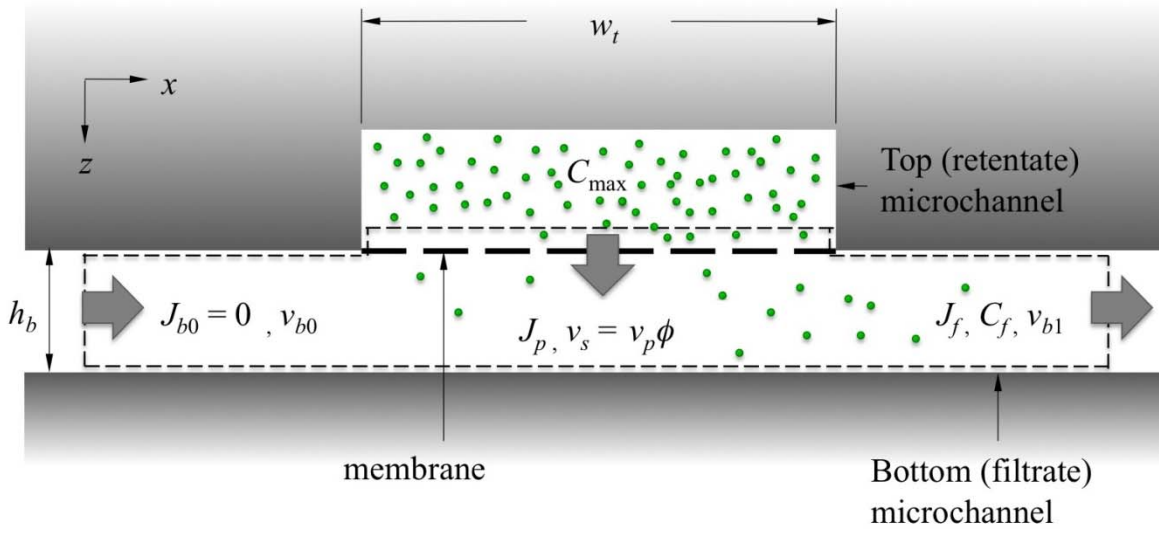

Figure S-2. Cross-sectional view of crossing microchannels along the length of the bottom channel. A known maximum solute concentration C_{max} from the top channel is allowed to permeate through the membrane (dark dashed line) to the lower channel where it is diluted to the filtrate concentration C_f, and carried downstream with a solute flux of J_f. Mass balances for both fluid and solute are applied to the control volume (dotted line).

$$c(z) = K_1 \exp\left(\frac{f_c}{f_d}\frac{v_p z}{D_s}\right) + \frac{J_p}{f_c v_p} \tag{S.2}$$

where K_1 is a constant of integration. The relevant boundary conditions for Eq. (S.**2**) include the solute concentration on the retentate side, C_{max} at z = 0 (i.e., top side of membrane), and the solute concentration on the filtrate side, C_f at $z = \delta$ (i.e., bottom side of membrane), where δ is the porous layer thickness. The solution to Eq. (S.**2**) is therefore:

$$J_p = f_c \times v_p C_{max}\left[\frac{1 - C_f/C_{max}\exp(\text{-Pe}_p)}{1 - \exp(\text{-Pe}_p)}\right] \tag{S.3}$$

where Pe_p is the pore Peclet number, defined as

$$\mathrm{Pe}_p = \left(\frac{f_c}{f_d}\right)\left(\frac{v_p \delta}{D_s}\right) \tag{S.4}$$

Eq. (S.**3**) accounts for both diffusive and convective flux, and the significance of each term is dependent on the magnitude of Pe_p (i.e., convection is dominant for $\mathrm{Pe}_p >> 1$, and diffusion is dominant for $\mathrm{Pe}_p << 1$). In all our experiments, $200 < \mathrm{Pe}_p < 500$, so Eq. (S.**3**) can be simplified to:

$$J_p = f_c \times v_p C_{\max} \tag{S.5}$$

Using similar arguments, we can derive an equation for solute flux of the filtrate in the bottom microchannel, J_f, where the applied bottom channel flow rates lead to channel Peclet numbers of $\mathrm{Pe}_c > 10^4$. Thus, we have

$$J_f = v_{b1} C_f \tag{S.6}$$

where v_{b1} is the average velocity of the filtrate in the bottom microchannel, *downstream of the membrane*. Solute flux of the filtrate results from the dilution of permeated solute molecules by the portion of buffer stream in the bottom microchannel *upstream of the membrane*, which initially contains no solute.

To relate C_f and $C_{\max}$ in terms of system parameters and pore velocity, continuity of both the fluid and the solute species are considered, resulting in the following mass balance equations (see Figure S-2):

$$v_{b1} A_b = v_{b0} A_b + v_p A_m \phi \tag{S.7}$$

and

$$J_f A_b = J_p A_m \phi \tag{S.8}$$

$A_m = w_t w_b$ is the total membrane area separating top and bottom microchannels, and is the product of the microchannel widths at the channel intersection; $A_b = w_b h_b$ is the bottom channel cross-sectional area; and ϕ is the porosity of the membrane. Combining Eqs. (S.**5**) and (S.**8**), we obtain an equation for the concentration ratio $\overline{C}$:

$$\overline{C} = \frac{C_f}{C_{\max}} = \frac{f_c v_p \phi A_m}{v_p \phi A_m + v_{b0} A_b} = \frac{f_c v_s w_t}{v_s w_t + v_{b0} h_b} \tag{S.9}$$

In Eq. (S.**9**), we have used the definition for superficial velocity, $v_s = v_p \phi$, a term commonly used in porous media flow because of its classical treatment in Darcy's law. Eq. (S.**9**) can be rearranged to give a formula for v_s in terms of the concentration ratio:

$$v_s = v_{b0} \frac{h_b}{w_t} \cdot \frac{\overline{C}}{f_c - \overline{C}} \tag{S.10}$$

Eq. (S.**10**) is an important formula for our fluorescence-based approach because it demonstrates that superficial velocity can be predicted from just system parameters (v_{b0}, h_b, w_t, f_c) and experimental measurements of $\overline{C}$ alone. With respect to our detection method, fluorescence intensity (FI) detected on the filtrate side is normalized to the maximum FI located uniformly on the retentate side, yielding a relative FI value that is equivalent to the ratio of solute concentrations between the two sides, $\overline{C}$.

As mentioned above, fluid flow through porous media is governed by the classical Darcy's Law, which relates the pressure drop across a porous layer to the superficial velocity of the bulk fluid,[2]

$$v_s = \frac{k}{\mu} \frac{\Delta p_T}{\delta} \tag{S.11}$$

where k is the specific permeability; μ is the dynamic viscosity of the fluid; and Δp_T is the transmembrane pressure. Δp_T can be determined by considering the mid-length pressures

in the top and bottom microchannels, $p_{t,m}$ and $p_{b,m}$ respectively, based on the applied flow rates in both channels and the assumption that pressure decreases linearly along both lengths. Because the microchannels have rectangular cross-sections, the velocity profiles in top and bottom microchannels, $v_t(x,z)$ and $v_b(y,z)$ respectively, can be approximated by the Purday approximation.[3] For example, for the bottom microchannel velocity profile, we have:

$$v_b(y,z) = v_{b0}\left(\frac{m+1}{m}\right)\left(\frac{n+1}{n}\right)\left[1-\left(\frac{2y}{w_b}\right)^m\right]\left[1-\left(\frac{2z}{h_b}\right)^n\right] \tag{S.12}$$

where m and n are empirical parameters dependent on channel aspect ratio $\alpha = h/w$. For $\alpha < 1/3$, $m = 1.7 + 0.5\alpha^{-1.4}$, and $n = 2$. By simplifying the Navier-Stokes equation for steady incompressible flow at low Reynolds number, the pressure gradient can be related to the second derivative of the velocity, and thus the pressure drop along the length of the microchannel can be written as:

$$\Delta p_b = 4\left(\frac{m+1}{m}\right)\left(n^2-1\right)\frac{\mu v_{b0} L_b}{h_b^2} = \frac{12\mu v_{b0} L_b}{h_b^2}\left(\frac{m+1}{m}\right) \tag{S.13}$$

Note that Eq. (S.**13**) has the familiar form of the pressure drop for steady laminar flow between infinite parallel plates, with the addition of the $(m+1)/m$ term to account for side wall effects. A similar equation can also be derived for pressure drop in the top microchannel. The pressures at the channel mid-lengths $L_t/2$ and $L_b/2$ can then be determined, yielding the following formula for Δp_T:

$$\Delta p_T = p_{t,m} - p_{b,m} = 6\mu\left(\frac{L_t v_t}{h_t^2} - \frac{L_b v_{b0}}{h_b^2}\right)\left(\frac{m+1}{m}\right) \tag{S.14}$$

With this relationship for Δp_T, and the formula relating v_s to $\overline{C}$, a closed-form solution for specific permeability can be written by combining Eqs. (S.**10**), (S.**11**), and (S.**14**):

$$k = \frac{1}{6}\left[\frac{\overline{C}}{f_c - \overline{C}}\right]\left[\frac{h_t^2 h_b^3 \delta}{w_t}\right]\left[\frac{v_{b0}}{L_t v_t h_b^2 - L_b v_{b0} h_t^2}\right]\left[\frac{m}{m+1}\right] \quad \text{(S.15)}$$

The significance of Eq. (S.**15**) lies in the fact that k can be determined by only measuring $\overline{C}$, since all other variables are known system parameters.

Finally, we discuss steric and viscous effects that determine f_c for the porous layer. Each of the secondary effects, f_{steric} and $f_{viscous}$, reduces the theoretical flux through the pores independently, and the combined effect through their product yields the total effect of f_c:

$$f_c = f_{steric} \times f_{viscous} \quad \text{(S.16)}$$

The steric effect refers to the finite molecular size of the solute, which effectively reduces the available pore area for solute flux by an amount related to the solute radius, s,[1]

$$f_{steric} = \left(\frac{r_p - s}{r_p}\right)^2 \quad \text{(S.17)}$$

Eq. (S.**17**) is the ratio between available pore area for solute flux and actual pore area for fluid flow, where r_p is the pore radius.

The viscous effect refers to the hydraulic resistance of the small pores to the finite-sized solute molecules, and can be approximated by the formula derived by Faxen,[1]

$$f_{viscous} = 1 - 2.104\frac{s}{r_p} + 2.09\left(\frac{s}{r_p}\right)^3 - 0.95\left(\frac{s}{r_p}\right)^5 \quad \text{(S.18)}$$

The variables and known system parameters used in this derivation are summarized in Table S.1 below.

Table S.1. Reference List of Variables and Measured System Parameters

Parameter	***Symbol***	***Value***	***Units***
Microchannels			
Microchannel height	$h = h_t = h_b$	120	μm
Microchannel width	$w = w_t = w_b$	800	μm
Top microchannel length	L_t	25	mm
Bottom microchannel length	L_b	50	mm
Bottom channel cross-sectional area	$A_b = w_b h_b$	0.096	mm^2
Membrane			
Membrane thickness	δ	11	μm
Pore density (manufacturer specifications)	N_0	16,000	$pores/mm^2$
Pore density (SEM image)	N_0	17,700	$pores/mm^2$
Porosity (SEM image)	ϕ	0.0169	[1]
Pore radius (manufacturer specifications)	r_p	0.5	μm
Pore radius (SEM image)	r_p	0.537 ± 0.043	μm
Membrane area	$A_m = w_b w_t$	0.64	mm^2
Fluid and Solute Properties			
Dynamic fluid viscosity	μ	0.001	$N{\cdot}s/m^2$
Solute diffusivity (FITC-BSA)[4]	D_s	60.7×10^{-6}	mm^2/s
Solute radius[5]	s	3.5	nm
Empirical Constants			
Diffusive flux ratio, pore-to-free solution	f_d	-	[1]
Convective flux ratio, pore-to-free solution	f_c	0.973	[1]
Viscous effect factor	$f_{viscous}$	0.986	[1]
Steric effect factor	f_{steric}	0.987	[1]
Empirical constant, Purday approx.	m	8.82	[1]
Empirical constant, Purday approx.	n	2	[1]
Other Variables			
Solute concentration	$c = c(z)$		mol/m^3
Filtrate concentration	C_f		mol/m^3
Maximum concentration	$C_{\max}$		mol/m^3
Concentration ratio	$\overline{C}$		[1]
Bottom channel velocity, *upstream of membrane*	v_{b0}		m/s
Bottom channel velocity, *downstream of membrane*	v_{b1}		m/s
Superficial velocity	v_s		m/s
Pore velocity	v_p		m/s
Solute flux, pore	J_p		$mol/(m^2 s)$
Solute flux, free solution	J		$mol/(m^2 s)$
Pore Peclet number	Pe_p		[1]
Channel Peclet number	Pe_c		[1]
Transmembrane pressure	Δp_T		Pa
Mid-length pressure, top channel	$p_{t,m}$		Pa
Mid-length pressure, bottom channel	$p_{b,m}$		Pa
Measured permeability	k		m^2
Theoretical permeability	k_0		m^2
Percentage error	E		%

Comparison of Theory and Experiment

The derivation above shows how permeability can be determined from experimental LIF measurements of solute concentration. To validate the accuracy of our derivation and the predicted permeability values determined by this method, we compared the measured value of permeability for an untreated plain track-etched membrane to a theoretical estimate of permeability, based on the cylindrical pore flow model.

Cylindrical Pore Flow Model

Track-etched membranes consist of a parallel arrangement of straight cylindrical pores that individually act as fluid conduits. For a single pore, the flow rate through the pore, q, is governed by the Hagen-Poiseuille law:

$$q = -\frac{\pi r_p^4}{8\mu}\frac{dp}{dz} \tag{S.19}$$

Multiplying the flow rate for a single pore by the pore density of the membrane N_0, we obtain the superficial velocity similarly defined in Darcy's law:

$$v_s = N_0 q = -\frac{N_0 \pi r_p^4}{8\mu}\frac{dp}{dz} \tag{S.20}$$

Comparing Eq. (S.**20**) to Eq. (S.**11**) shows that theoretical permeability based on the cylindrical pore flow model, k_0, can be written as

$$k_0 = \frac{N_0 \pi r_p^4}{8} \tag{S.21}$$

Thus, a theoretical estimate of permeability can be determined by measuring pore density and pore radius of the membrane.

Scanning Electron Microscopy

Scanning electron microscopy was used to acquire an image of the membrane surface for determining pore density and pore radius (**Figure S-3**A). Image analysis (ImageJ, NIH) showed pore density N_0 = 17,700 pores/mm^2, and pore radius r_p = 0.543 ± 0.093 μm (**Figure S-3**B), with one outlier (r_p = 1.67 μm) as confirmed by Grubbs' test[6] (P<0.01). These values are comparable to manufacturer's specifications (N_0 = 16,000 pores/mm^2; r_p = 0.50 μm), but are ~10% larger for both values.

Error Analysis

We compared measured and theoretical permeability values based on our measurements of membrane properties and fluorescence detection of solute concentration. We were interested in analyzing the sensitivity of the model to changes in membrane properties, specifically differences in pore radius from manufacturer specifications to measured values, and the effect of including secondary steric and viscous effects in the calculations.

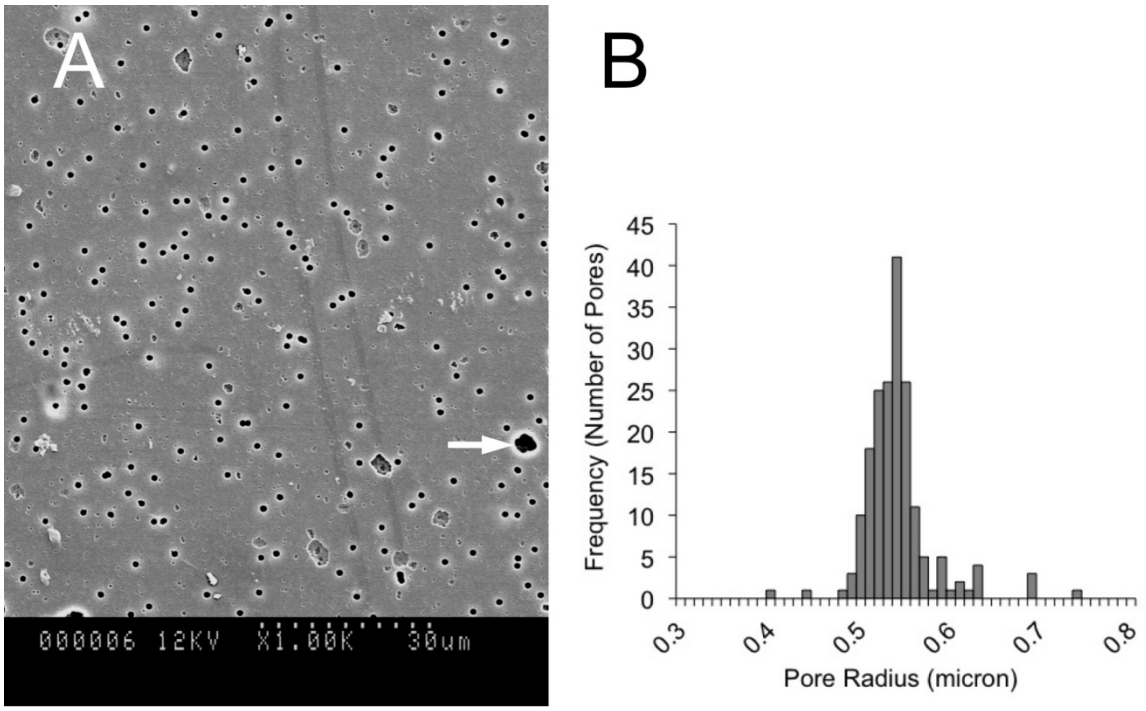

Figure S-3. (A) Image of top view of track-etched PET membrane obtained by scanning electron microscopy. White arrow indicates outlier in pore distribution. (B) Histogram showing distribution of pore radii.

Percentage error was calculated by using the measured *k* values as reference:

$$E = \left| \frac{k - k_0}{k} \right| \times 100\% \qquad \text{(S.22)}$$

The results of the error analysis are summarized in Table S.2. Manufacturer specifications were found to be inadequate for providing an accurate theoretical value to validate our measured values. Using pore radius obtained from scanning electron microscopy vastly reduced the discrepancy between measurement and theory. By including steric and viscous effects, we found that our model and measurements were in excellent agreement, with less than 1% error between theory and measurement.

Table S.2. Error between Measured and Theoretical Permeability Values

		Theoretical k_0 (10^{-10} mm^2)	
		Manufacturer specifications	*Measured pore parameters*
***Measured k* (10^{-10} mm^2)**		*3.93*	*5.77*
No secondary effects	*5.43*	**27.6%**	**6.3%**
With secondary effects	*5.73*	**31.4%**	**0.7%**

References

1. Friedman, M.H. Principles and models of biological transport. (Springer, New York, NY, USA; 2008).
2. Scheidegger, A.E. The physics of flow through porous media. (University of Toronto Press, Toronto, Canada; 1974).
3. Shah, R.K. & London, A.L. Laminar flow forced convection in ducts. (Academic Press, New York; 1978).
4. Muramatsu, N. & Minton, A.P. tracer diffusion of globular-proteins in concentrated protein solutions. *Proc. Natl. Acad. Sci. U. S. A.* **85**, 2984-2988 (1988).
5. Fu, B.M.M. & Shen, S. Structural mechanisms of acute VEGF effect on microvessel permeability. *American Journal of Physiology-Heart and Circulatory Physiology* **284**, H2124-H2135 (2003).
6. Grubbs, F.E. Procedures for detecting outlying observations in samples. *Technometrics* **11**, 1-21 (1969).